Reducing Surface Halide Deficiency for Efficient and Stable Iodide-Based Perovskite Solar Cells

Wu-Qiang Wu^{a,b#}, Peter N. Rudd^{a#}, Zhenyi Ni ^a, Charles Henry Van Brackle^a, Haotong Wei^a, Qi Wang^a, Benjamin R. Ecker^c, Yongli Gao^c, Jinsong Huang^{*a}

a Department of Applied Physical Sciences, University of North Carolina, Chapel Hill, NC 27599, USA

b Nanomaterials Centre, School of Chemical Engineering and Australian Institute for Bioengineering and Nanotechnology, The University of Queensland, Brisbane, QLD 4072, Australia.

c Department of Physics and Astronomy, University of Rochester, Rochester, NY 14627, USA

Abstract: State-of-the-art, high-performance perovskite solar cells (PSCs) contain a large amount of iodine to realize smaller bandgaps. However, the presence of numerous iodine vacancies at the surface of the film formed by their evaporation during the thermal annealing process has been broadly shown to induce deep-level defects, incur non-radiative charge recombination and induce photocurrent hysteresis, all of which limit the efficiency and stability of PSCs. In this work, modifying the defective surface of perovskite films with cadmium iodide (CdI₂) effectively reduces the degree of surface iodine deficiency, and stabilizes iodine ions via the formation of strong Cd-I ionic bonds. This largely reduces the interfacial charge recombination loss, yielding a high efficiency of 21.9% for blade-coated

1

[#] Contributed equally to this work

PSCs with an open-circuit voltage of 1.20 V, corresponding to a record small voltage deficit of 0.31 V. The CdI₂ surface treatment also improves the operational stability of the PSCs, retaining 92% efficiency after constant illumination at 1 sun intensity for 1000 h. This work provides a promising strategy to optimize the surface/interface optoelectronic properties of perovskites for more efficient and stable solar cells and other optoelectronic devices.

INTRODUCTION

The certified power conversion efficiencies (PCEs) of perovskite solar cells (PSCs) have recently exceeded 25.0%, already surpassing crystalline silicon solar cells, thus becoming the forefront of photovoltaic technologies and attracting intense research interest worldwide. To date, state-of-the-art PSCs with efficiencies over 21% are mainly achieved by employing a cesium (Cs), rubidium (Rb), methylammonium (MA) and formamidinium (FA) mixed-cation perovskite in combination with high ratios of iodide.² In solution-processed perovskites, several types of deep-level defects, such as vacancies, are easily formed at the surface of polycrystalline perovskite films.³⁻⁵ These halide vacancies at the surface instigate interfacial charge recombination, resulting in detrimental influences over carrier dynamics and incurring photocurrent hysteresis in PSCs. 6-11 In addition, the diffusion of ionic vacancies is normally accompanied by the migration of other cations or anions, which facilitates the irreversible chemical decomposition of perovskite and limits the long-term stability of PSCs. 12,13 Reducing the degree of halide deficiency via effective defect engineering or chemical modulation is ultimately beneficial to achieving further improvements in the performance and stability of PSCs.

Several strategies have been reported to effectively fill or suppress the formation of the iodide vacancies. 14-19 For instance, excess iodide ions have been incorporated into the organic cation solution of a two-step deposition method in order to compensate for the loss of halide anions during the thermal processing stage and decrease the number of iodide vacancies in the perovskite layer.¹⁴ Alternatively, some metal or ammonium halides have demonstrated the capability to suppress the formation of iodide vacancies, and/or achieve multi-vacancy defect passivation via the formation of hydrogen bonds, 15,16 ionic bonds 17,18 or lattice strain relaxation. 19,20 However, these strategies mainly focus on healing halide vacancies by supplying excess halide ions in the bulk perovskite film. Under thermal annealing conditions, halide vacancies are readily formed at the surface of the resultant polycrystalline perovskite films because of the small chemical bonding energy of Pb-I (142 kJ mol⁻¹), and the volatility of I₂ and methylammonium iodide (MAI). 19,21-23 Due to halide vacancies at the surface resulting in losses through interfacial nonradiative charge recombination, even a small density of halide vacancies can be highly detrimental to device performance. To overcome these challenges, an ideal way is to fill the iodide vacancies using a second coating of excess iodine ions on the perovskite film surface, while at the same time immobilizing these halide ions via formation of stronger chemical bonds.

We report a strategy to both reduce the perovskite surface iodide deficiency and suppress the surface iodide vacancy formation via a simple treatment with cadmium iodide (CdI₂). The surface iodide vacancies are effectively filled by CdI₂ and incorporated Cd²⁺ ions, to a large extent, prevent the loss of iodide ions owing to the formation of Cd-I ionic bonds with stronger bonding energy, relative to Pb. This surface modification strategy resulted in significantly enhanced efficiency and stability of blade-coated PSCs, achieving a high, stabilized open-circuit

voltage (V_{oc}) up to 1.20 V, corresponding to a record small V_{oc} deficit of 0.31 V. The resultant PSCs with CdI₂ surface treatment exhibited excellent long-term operational stability with 92% of their original PCE retained after 1000 h of continuous 1 sun illumination. Incorporation of a relatively large amount of Cd²⁺ ions (2.0 mol%) into mixed cations perovskite has been demonstrated to reduce the lattice strain throughout the bulk perovskite film for improved stability.¹⁹ Distinguished from this, we aimed to employ an effective surface treatment with only 300 ppm of CdI₂ to reduce the detrimental surface halide deficiencies of iodide-based perovskite films via synergistic functions of both filling the halide vacancies for reduced interfacial recombination loss and immobilizing the halide anions for enhanced operational stability, which is beneficial to improve both the efficiency and stability of the blade-coated PSCs.

RESULTS AND DISCUSSION

In this study, we employed a perovskite composition with quadruple cations of Rb⁺, Cs⁺, FA⁺ and MA⁺ due to its optimal bandgap and excellent optoelectronic performance.² The control perovskite films were fabricated via a previously reported one-step blade-coating method.²⁴⁻²⁶ Once the perovskite film was prepared, a facile CdI₂-coating strategy was applied, whereby 0.3 mg mL⁻¹ CdI₂ dissolved in isopropyl alcohol (IPA, a common antisolvent for perovskite), was spin-coated on top of the perovskite film followed by thermal annealing. We propose the most plausible working mechanisms for how the CdI₂ surface treatment can reduce the surface halide deficiency of blade-coated perovskite films, as illustrated in Figure 1. First, isovalent Cd²⁺ has a smaller ionic radius (95 pm) than Pb²⁺ (119 pm), and therefore could be homogeneously incorporated into the bulk of mixed cation perovskite by partially substituting the Pb²⁺ ions, thus forming a highly stable perovskite structure (i.e., with a tolerance factor close to 1).²⁷ The successful incorporation of Cd within the local lattice of perovskite has been confirmed in a

perovskite single crystal with Cd/Pb atomic ratio of 0.08.19 When less than 5 mol% Cd was added to the perovskite ink, the main (110) characteristic X-ray diffraction peak of the resulting thin films shifted to a higher 20 position, relative to the control, implying the successful incorporation of Cd into the perovskite crystal lattice (Figure S1). The blurred (110) peak with two tips may indicate phase segregation, a phenomenon normally seen in mixed cation perovskite films containing Rb and Cs ions.²⁸ Additionally, excessive Cd (>10 mol% relative to Pb) results in lattice expansion, which can be explained by the accumulation of Cd at the lattice interstitial sites (Figure S1). However, surface treatment of perovskite films by a small amount of CdI₂ (i.e. 0. 3 mg/mL in IPA, spin-coated at a speed of 6000 rpm) shows no apparent change in the crystalline structure or orientation (Figure S2). It is worth pointing out the use of a dynamic spin coating method at 6000 rpm with just 0.3 mg/mL CdI₂ solution results in the introduction of very little Cd, but provides vast improvements in efficiency and stability. Additionally, considering the encapsulation of devices in future commercialized products, the minuscule amount of Cd present shouldn't cause any more of a problem than the Pb in the film. The bond energy of the formed Cd-I ionic bond was stronger than that of the Pb-I counterpart owing to the larger electronegativity difference between Cd and I. In this case, the surface iodide is more difficult to evaporate and is thus better stabilized. The second way the CdI₂ surface treatment reduces the surface halide deficiency of blade-coated perovskite films is by filling the surface iodide vacancies by supplying excess iodide ions. Third, the Cd ion can serve as appropriate B-site anion, which could effectively suppress the formation energy of iodide vacancies by ≥0.5 eV. 19 Overall, the beneficial roles of CdI₂ surface treatment can be summarized as filling the surface halide vacancies, immobilizing the halide anions, and suppressing vacancy formation.

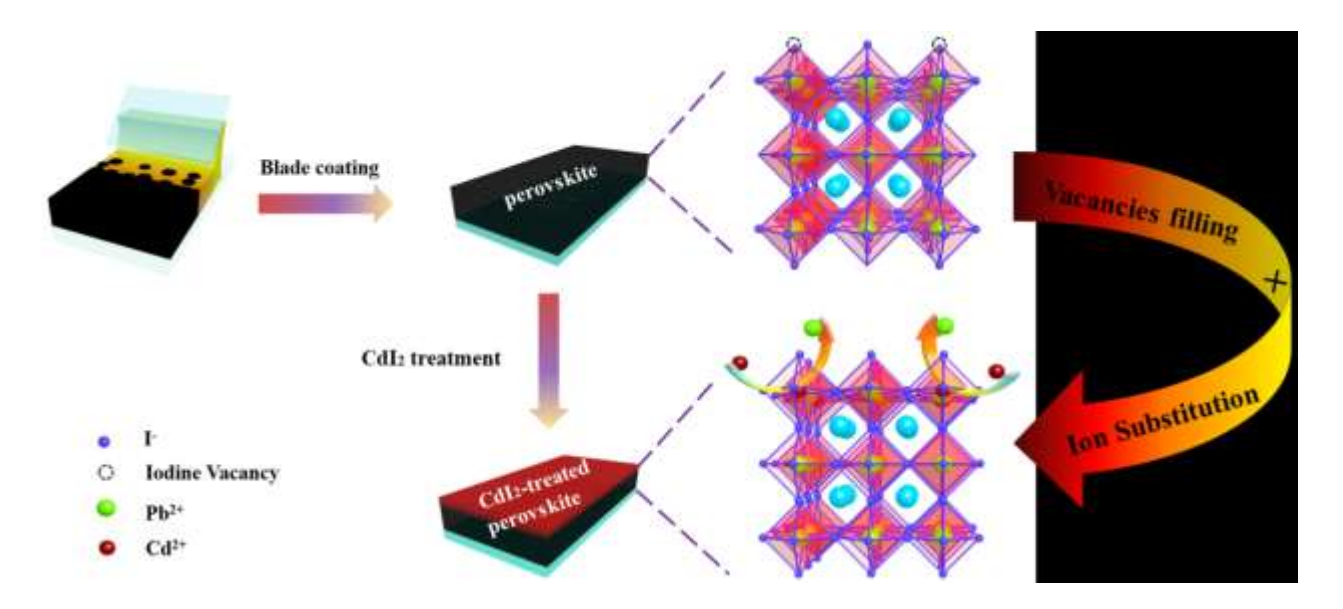


Figure 1. A schematic illustration of a blade-coated perovskite film with CdI₂ surface treatment. Note: The perovskite film was blade-coated on a pre-heated ITO substrate. For CdI₂ surface treatment, the CdI₂/IPA solution with various concentrations (0.3 mg/mL, 0. 6 mg/mL and 01.2 mg/mL) was dynamically spin-coated on top of the as-prepared perovskite film.

We carried out an X-ray photoelectron spectroscopy (XPS) study to investigate the effect of CdI₂ modification on the surface composition. XPS is a surface sensitive technique, which is normally used to characterize only the top 5 nm of a material.²⁹ We intentionally measured three spots on each film surface, and at least three films were measured for each condition to ensure the reliability of the results. High-resolution spectra of Pb 4f, I 4d, and Cd 3d regions are shown in Figure S3. The XPS result shows the presence of Cd (Cd/Pb atomic ratio is ~0.14%) on the surface of the CdI₂-treated perovskite film. By normalizing the spectra with respect to the Pb 4f peak, we compared the I/Pb ratio between control and CdI₂-treated films. In a pure iodide-based control perovskite, the bulk material theoretical I/Pb stoichiometric value should be close to 3. However, the average I/Pb ratio for the pristine control perovskite film from the XPS

measurement was just 2.33, indicating that an iodide-deficient characteristic exists in the neat perovskite film surface made by blading process. After CdI₂ surface treatment, the average I/Pb ratio at the surface had a statistically relevant increase to 2.85, suggesting that iodide vacancies on the surface had been effectively filled by the CdI₂ treatment (Figure 2a). Even considering the Cd²⁺ ions can replace the Pb²⁺ ions to some extent, the I/(Pb+Cd) ratio at the surface has reached ~2.50, which is high than the I/Pb ratio in the pristine perovskite films without CdI₂ treatment. Surface treatment by CdI₂ thus mitigates the loss of iodide during the thermal annealing process of perovskite film fabrication. Through improving the I/Pb ratio, the number of vacancies and traps responsible for the detrimental capture of charge carriers during carrier generation and charge transport processes is effectively reduced.

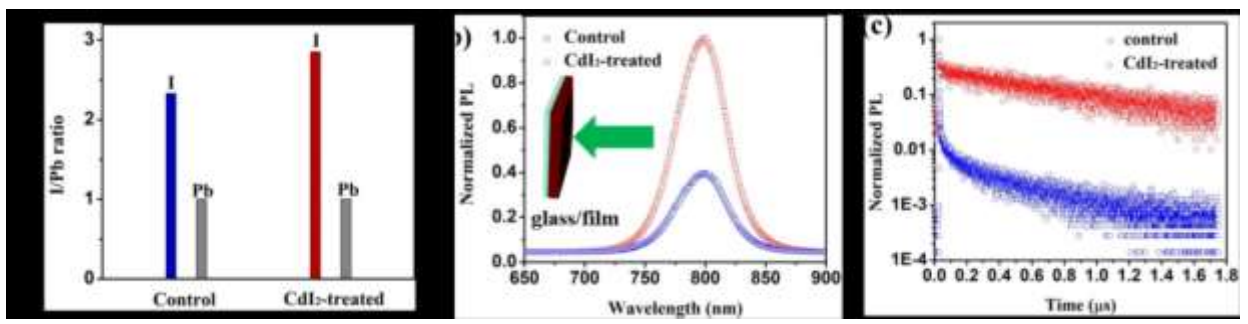


Figure 2. (a) Relative I/Pb ratio at the surface of control and CdI₂-treated perovskite films calculated from the XPS measurements. (b) PL spectra and (c) TRPL lifetime of the control and CdI₂-treated perovskite films emitted from the film side (i.e. excitation of the top surface).

To gain more insight into charge-carrier recombination dynamics with the change of electronic states, we monitored the steady-state photoluminescence (PL) spectroscopy and time-resolved PL (TRPL) intensity decay of the glass/perovskite films with or without CdI₂ surface treatment. The top surface of the CdI₂-treated film exhibited a stronger PL emission (~3 fold enhancement) relative to the untreated films at the same excitation intensity (Figure 2b).

Since perovskite materials absorb strongly at short wavelengths, we anticipated that only the surface of the films (depth <100 nm) was excited by the 532 nm laser. Hence, the significantly enhanced PL intensity indicates that CdI₂ treatment largely suppressed the surface non-radiative recombination.³⁰ We also observed enhancement of PL intensity for the bottom surface of the CdI₂-treated film (Figure S4), despite the treatment being mainly on the film surface. This can be possibly attributed to the diffusion of iodide and/or Cd²⁺ ions along the grain boundaries during thermal annealing process, which could also reduce halide vacancies at the bottom surface of perovskite films. Transient PL decay provides insight into charge recombination via non-radiative tunnels related to defect concentration. 14,31 The TRPL profiles were fitted with bi-exponential decays for both control and CdI₂-treated films. The relatively fast decay component (τ_1) was assigned to the charge trapping process, while the much slower decay component (τ_2) was assigned to the de-trapping or carrier recombination processes.³² It is noted that the excitation intensity from the laser was very weak, which only generated a carrier density of 10¹³-10¹⁴ cm⁻³ per laser pulse in the DeltaFlex TCSPC system, meaning the PL transients should exhibit trapping behavior. A larger, faster initial decay in light intensity immediately after light excitation indicates a large number of photogenerated charges are quickly trapped by a high density of trap states. These trapped charges can recombine through nonradiative processes or be reemitted to their respective bands. Treatment by CdI₂ increased τ_1 from 0.4 ns to 1.2 ns, suggesting a slower trapping process due to a lower density of available charge trap states. In addition, we can estimate what percentage of charges are trapped by observing the magnitude of the initial PL drop due to charge trapping. The control perovskite film sees its PL signal reduced by nearly 98% during the relatively fast decay process (in Figure 2c, the PL decays nearly two orders of magnitude in the fast decay), indicating that virtually all the charges are trapped shortly

after photogeneration. In the perovskite film treated with CdI₂, we only see a PL reduction of approximately 70% in the same time frame, suggesting that far fewer charges are trapped. This result implies that the charge trapping in CdI₂-treated films was greatly suppressed, which can be attributed to the decreased number of surface vacancy defects after the CdI₂ treatment.³³

To investigate the influence of CdI₂ treatment on photovoltaic performance, we fabricated *p-i-n* planar PSCs with the following architecture: ITO/HTL/perovskite/ETL/Cu (Figure S5), where ITO is indium-doped tin oxide, HTL is the hole transport layer made of poly[bis(4-phenyl)(2,4,6-trimethylphenyl)amine(PTAA), ETL is the electron transport layer made of C₆₀ and bathocuproine (BCP, hole blocking layer). The thickness of the perovskite absorber layer is approximately 600 nm (Figure S6). We first investigated the dependence of the device performance on the CdI₂ solution concentration. The PCE increased significantly with the maximum performance attained when the perovskite films were treated with the 0.3 mg/mL CdI₂/IPA solution. The device performance began to drop when the CdI₂ concentration increased to 0.6 mg/mL, and was very poor at higher concentrations, possibly owing to insulation by CdI₂ (Figure 3a, Figure S7and Table S1).

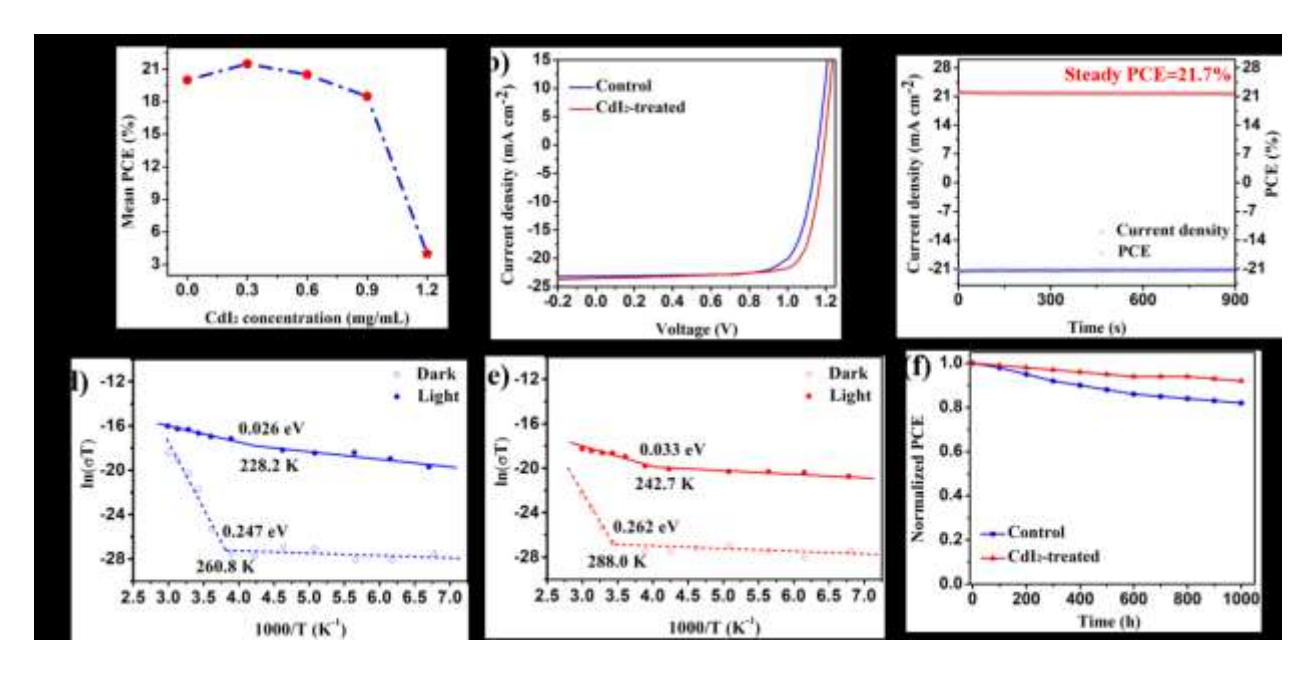


Figure 3. (a) Relationship between mean PCE and the surface treatment CdI₂ concentration. (b) *J-V* curves of PSCs with or without CdI₂ treatment. (c) Stabilized current density and PCE at the maximum power point (1.0 V) of the champion device based on the CdI₂-treated perovskite film. Temperature-dependent conductivity of the perovskite films (d) without and (e) with CdI₂ surface treatment. (f) Operational stability of encapsulated PSCs with or without CdI₂ treatment under continuous 1 sun illumination.

Table 1| Photovoltaic parameters of PSCs based on RbCsFAMAPbI₃ perovskite (with an energy band gap (E_g) of 1.51 eV) with or without CdI₂ treatment under 1 sun illumination (AM 1.5G, 100 mW cm⁻²).

PSCs	J_{sc}	V_{oc}	η	Average η	FF	V _{oc} deficit
	mA cm ⁻²	/V	/%	/%	/%	/V
Control	23.1	1.16	20.2	19.12±1.08	75.2	0.35

[*] data for the average PCE (η) were calculated from at least 30 devices.

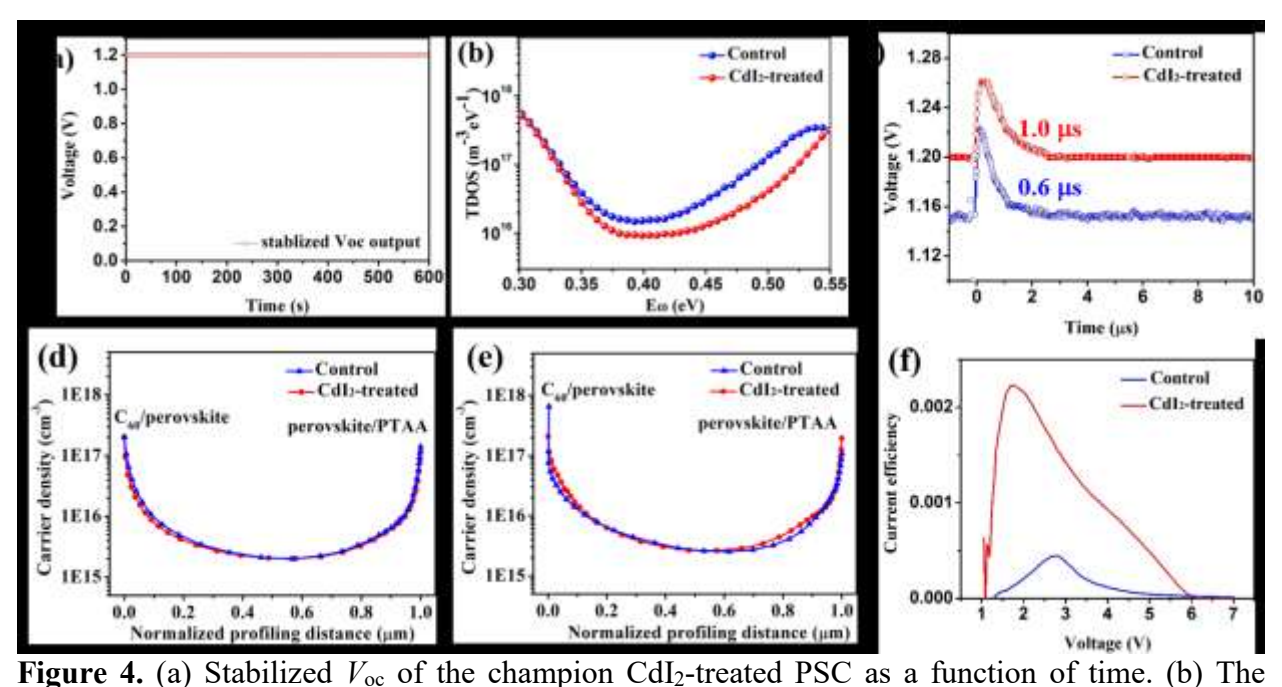
The typical J-V curves of the devices with or without 0.3 mg/mL CdI₂ surface treatment are shown in Figure 3b and the corresponding photovoltaic parameters are summarized in Table 1; CdI₂ treatment of the perovskite surface produced an obvious improvement in device performance. The optimized control device without CdI₂ treatment exhibited an efficiency of 20.2%. In comparison, the optimized CdI₂ treated device achieved an efficiency of 21.9%, along with a $V_{\rm oc}$ as high as 1.20 V, a short-circuit current density ($J_{\rm sc}$) of 23.5 mA cm⁻² and a fill factor (FF) of 77.7% (Figure 3b), with negligible J-V hysteresis (Figure S8 and Table S2). Devices with CdI_2 treatment showed only a slight increase in J_{sc} , as seen by the nearly overlapping external quantum efficiency (EQE) spectra when compared to the control device. In addition, the integrated $J_{\rm sc}$ values from the EQE spectra coincided well with values acquired from the J-Vresults, with <3% discrepancy (Figure S9). The greatest photovoltaic parameter enhancements were for V_{oc} and FF. We attribute this improvement to the reduction of surface halide vacancy defects (e.g. iodide) by CdI₂ treatment, which enabled better suppression of interfacial charge recombination.³⁴⁻³⁶ The best CdI₂-treated device was held and measured at a maximum power point (MPP) of 1.0 V, stabilizing within seconds, yielding a stabilized power output of 21.7% under AM 1.5G illumination (Figure 3c). The statistics of the PCE distribution confirm that CdI₂-treated devices had consistently better performance and exhibited higher reproducibility (Figure S10). Defects in perovskites normally induce degradation of the perovskite films, leading to deterioration of device performance under illumination.³⁷ Control and engineering of the formation and migration of vacancy defects at the perovskite surface is crucial to improving both

the performance and stability of PSCs. Surface treatment by CdI₂ proves capable of supplementing the deficiency of I⁻, but we also believe the strong interaction between I⁻ and Cd²⁺ is capable of immobilizing ions to suppress ion migration at the film surface and thus is beneficial to improve operational stability. Using temperature-dependent conductivity study, the activation energy for ion migration (E_a) was calculated using the Nernst-Einstein relation, described in our previous reports.^{38,39} Under dark conditions, we found the conductivity of the control film is dominated by ionic conductivity at a temperature of 260.8 K with an E_a of 0.247 eV. Treatment with CdI₂ effectively increases the activation temperature in the dark to 288.0 K and an E_a to 0.262 eV (Figure 3d and 3e). As expected, the introduction of a 20 mW cm⁻² light bias reduces the activation temperature and E_a of both samples; however, the CdI₂-treated films again exhibit a higher activation temperature and E_a , relative to the control (Figure 3d and 3e). The increase of E_a with CdI₂ treatment confirms that the introduction of strong Cd-I interactions can effectively suppress ion migration to reduce the density of iodide vacancies and improve the stability of the perovskite materials. We investigated the stability of encapsulated PSCs under continuous AM 1.5G illumination. The photostability of the CdI₂-treated device was superior to that of the reference cell, maintaining 92% of the original PCE after 1000 h of illumination, while the control device only retained 82% of the initial PCE during the same illumination duration (Figure 3f). The extended stability of CdI₂-treated PSCs under operational condition can be attributed to a decreased concentration of mobile ionic vacancies or defects and the effective passivation of defects at the perovskite film surface to reduce the interfacial recombination losses.

An astonishing result achieved in this work is the $V_{\rm oc}$ as high as 1.20 V (stabilized for 10 min) for the CdI₂-treated device (Figure 4a), confirming the highly effective surface passivation with

treatment by CdI₂. Estimated from the EQE response onset at 821 nm (Figure S9), the optical bandgap of the control perovskite was determined to be ~1.51 eV. Hence, there is only an ~0.31 V $V_{\rm oc}$ loss for these PSCs, which is far less than crystalline silicon solar cells (0.38 V) and comparable to GaAs solar cells (0.30 V).⁴⁰ To the best of our knowledge, this is, to date, the record for smallest V_{oc} deficit reported for PSCs, regardless of fabrication method. To further examine the effects of CdI₂ treatment on the distribution of defects and recombination dynamics, comprehensive characterization was performed using admittance spectroscopy and transient photovoltage (TPV) decay. Admittance spectroscopy is a well-established method to quantify the trap density of states (tDOS) in thin-film photovoltaics.^{8,41} CdI₂ surface modification dramatically reduced the trap state density, particularly in the depth region of 0.40-0.55 eV, which corresponded to the defects at film surface (Figure 4b).8 This result confirms the beneficial role of CdI₂ treatment on reducing the surface defects, such as halide vacancies, which is favorable for suppressing interfacial recombination. The carrier recombination lifetime obtained from the TPV decay measurement increased from 0.6 µs in the control device to 1.0 µs for the CdI₂-treated device (Figure 4c), underscoring the necessity of surface vacancy defect reduction in suppressing interfacial charge accumulation and recombination, thus reducing charge transfer loss.⁴² In order to probe the carrier density throughout the profile of devices, drive-level capacitance profiling (DLCP) was used while applying alternating current (AC) frequencies of 100 kHz and 10 kHz. The carrier densities measured at the higher AC frequency of 100 kHz for the two films are basically the same, indicating that the CdI₂ surface treatment did not obviously change the doping concentration of the perovskite film (Figure 4d). On the contrary, at 10 kHz, CdI₂ treatment significantly reduces the carrier concentration at the perovskite/C₆₀ interface, indicative of a reduction in trap density (Figure 4e). As seen for the

CdI₂-treated perovskite films, the recombination dynamics are mainly dominated by a radiative recombination process. In general, a higher radiative recombination emission efficiency is responsible for achieving a higher $V_{\rm oc}$.^{43,44} We tested the PSC operating as a light emitting diode (LED) in the dark and under an applied electrical bias. The CdI₂-treated devices exhibited an almost 5-fold enhancement in terms of both current efficiency and brightness (Figure 4f and Figure S11), indicating that non-radiative pathways in the perovskite layer were largely suppressed, and that interfacial trap-assisted recombination had been significantly reduced by CdI₂ passivation. These inferences rationalize the extremely high $V_{\rm oc}$ with record small $V_{\rm oc}$ loss in blade-coated perovskite photovoltaics.



tDOS obtained from admittance spectroscopy measurement of the perovskite devices with or without CdI_2 treatment. (c) Carrier recombination lifetime measured by TPV. Dependence of the carrier density on the normalized profiling distance for PSCs based on control and Cd-treated perovskite films measured by DLCP at the AC frequency of (d) 100 kHz and (e) 10 kHz. (f) Current efficiency of the PSCs with or without CdI_2 treatment as a function of applied voltage

while operating as LEDs.

CONCLUSIONS

An effective isovalent metal halide surface treatment was developed to improve both the efficiency and stability of blade-coated PSCs based on mixed cations perovskite. The excess I from CdI₂ could effectively fill the iodide vacancies, while the small Cd²⁺ ions can partially substitute Pb²⁺ ions to form Cd-I interactions, with stronger ionic bonding character capable of suppressing the formation of halide vacancies. The CdI₂-treated PSCs made by blade-coating exhibited a high PCE of 21.9% (stabilized power output exceeding 21.7%). The reduced surface halide deficiency effectively decreased the density of defects at the surface and substantially suppressed non-radiative recombination, thus reducing the interfacial recombination loss to achieve a high V_{oc} of 1.20 V with a V_{oc} deficit of only ~0.31 V. The CdI₂ treatment retarded the ions/vacancies diffusion and dissociation, as well as immobilizing the halide anions, which together enhanced the operational stability of the blade-coated devices. This study opens a new avenue to mitigate surface point defects and manage halide anion deficiencies for the fabrication of high-efficiency, blade-coated PSCs with prolonged lifetime.

EXPERIMENTAL SECTION

Materials. Unless stated otherwise, all materials and solvents were purchased from Sigma-Aldrich. Lead iodide (PbI₂, 99.999%), rubidium iodide (RbI) and cesium iodide (CsI) were purchased from Alfa Aesar. Formamidinium iodide (FAI) and methylammonium iodide (MAI) were purchased from Greatcell Solar.

Device Fabrication. Prior to use, the cleaned ITO glasses (1.5 cm × 1.5 cm) were treated with UV-ozone (UVO) plasma for 15 min. The PTAA layer (~20 nm) and perovskite layer (~600 nm) were fabricated successively on the ITO glass via a blade-coating method.²⁴ The Rb_{0.025}Cs_{0.025}FA_{0.70}MA_{0.25}PbI₃ perovskite ink (1.2 M) was prepared by dissolving PbI₂, FAI, MAI, CsI and RbI into DMF (N,N-Dimethylformamide) solvent at the stoichiometry indicated. To achieve uniform coating of the perovskite film, small amounts of additives, e.g. methylammonium hypophosphite (MHP, 0.15 wt%), L-α-phosphatidylcholine (LP, 0.05 wt%), 1,3-diaminopropane (DAP, 0.025 wt%) were incorporated into the perovskite ink.^{24,25} For each coating, 5-10 µL of perovskite ink was bladed linearly at a speed of 7.5 mm s⁻¹ on a pre-heated ITO substrate. For the CdI₂-treated sample, the CdI₂/IPA solution at various concentrations (0. 3 mg/mL, 0.6 mg/mL and 1.2 mg/mL) was deposited on top of the freshly prepared perovskite film by dynamic spin coating at 6000 rpm for 30 s, followed by thermal annealing at 100 °C for 10 min. Finally, the device assembly was completed by sequential thermal evaporation of C₆₀ (Nano-C, ~25 nm), BCP (~8 nm) and Cu electrode (~80 nm). Lateral devices used in the temperature-dependent conductivity measurements were fabricated using similar methods by first depositing PTAA on glass followed by the perovskite layer, with or without CdI2 surface treatment. Devices were completed by thermally evaporating Au electrodes (65 nm) directly on the perovskite surface.

Device Characterization. Scanning electron microscopy (SEM) images were obtained using a Quanta 200 FEG environmental scanning electron microscope. X-ray diffraction (XRD) patterns were recorded with a Bruker D8 Discover Diffractometer with Cu Kα radiation (1.5406 Å). X-ray photoelectron spectroscopy (XPS) was conducted on a Kratos Axis Ultra DLD X-ray Photoelectron Spectrometer with a monochromatic Al K alpha source under high vacuum (10⁻⁹ mbar). The J-V measurement of the devices (voltage scanning rate 0.1 V s⁻¹) and the steady power output under maximum power output bias (1.0 V) were recorded with a Keithley 2400 source-meter under simulated AM 1.5G irradiation produced by a Xenon lamp solar simulator (Oriel Sol3A, Class AAA Solar Simulator). The light intensity was calibrated by a silicon reference cell equipped with a Schott visible color KG5 glass filter (Newport 91150V). A non-reflective shadow mask was used to define a 0.08 cm² active area of the PSCs. External quantum efficiency (EQE) spectra were measured by a Newport QE measurement kit by focusing a monochromatic light beam with wavelength from 300 nm to 850 nm onto the devices. Photoluminescence (PL) spectrum was measured with a Horiba iHR320 Imaging Spectrometer at room temperature. A 532 nm green laser (Laserglow Technologies) with an intensity of 100 mW cm⁻² was used as the excitation source. Time-resolved photoluminescence (TRPL) was obtained using a DeltaFlex TCSPC Lifetime Fluorometer with a pulsed laser source at 404 nm (Horiba DeltaDiode 405L; pulse width approximately 45 ps, 1 pJ per pulse and ~8 mm² spot size); the signal was recorded using time-correlated single photon counting (TCSPC). The DLCP and tDOS measurements were performed by using an Agilent E4980A precision LCR meter. For the DLCP measurement, the direct current (DC) bias was scanning from - 0.2 to 1.2 V for the PSCs.

And the amplitude of the AC biases (δV) were ranging from 20 to 200 mV. For each AC bias, an additional offset DC voltage was applied to keep the maximum forward bias constant. The measured capacitances (C) at each DC bias were gathered with a homemade computer program and fitted with a polynomial function to obtain C_0 and C_1 from the dependence of $C = C_0 + C_1 \delta V$ + $C_2(\delta V)^2$ + ... The carrier density (N) that includes both free carrier density and trap density is calculated by $N = -\frac{c_0^3}{2q\varepsilon A^2c_1}$ (where q is the elementary charge, ε is the dielectric constant of the semiconductor and A is the active area of the junction). The profiling distance from the junction barrier is given by $\varepsilon A/C_0$. For the tDOS measurement, the DC bias was fixed at 0 V and the amplitude of the AC bias was 20 mV. The scanning range of the AC frequency was 0.02 -2000 kHz. The tDOS $(N_T(E_{\omega}))$ is calculated by using an equation: $N_T(E_{\omega}) = -\frac{1}{akT}\frac{\omega dc}{d\omega}\frac{V_{bi}}{W}$, where W and V_{bi} are the depletion width and build-in potential, respectively, which were derived from the Mott-Schottky analysis of the C-V measurement. q, k, T, ω and C are elementary charge, Boltzmann's constant, temperature, angular frequency and specific capacitance, respectively. The demarcation energy $E_{\omega} = kT ln\left(\frac{\omega_0}{\omega}\right)$ (where ω_0 is the attempt-to-escape angular frequency that equals to $2\pi v_0 T^2$ (v_0 is the temperature-independent attempt-to-escape frequency)) is derived from the temperature-dependent C-f measurements which were carried out in a Lake Shore Cryotronics probe stage with a Lake Shore Cryotronics temperature controller model 336. Transient photovoltage (TPV) decay was measured under one sun illumination and recorded by a 1 GHz Agilent digital oscilloscope. Temperature-dependent conductivity measurements were carried out using a Lakeshore temperature-controlled probe station. A constant bias was applied to generate a small electric field fixed at 0.4 V/ μ m, and a light bias of 20 mW cm⁻² was applied

through a quartz window for light measurements. Current was measured until stabilized and ion migration activation energy was calculated using the Nernst-Einstein relation, using methods we have previously reported.³⁸ For the long-term photostability test under constant illumination from a 300 W plasma lamp at room temperature with an adjusted light intensity of 100 mW cm⁻², the devices were encapsulated with epoxy and glass slides. The encapsulated devices were connected to a resistor to make them operate at the MPP from the start of the stability test. The device might stay away from the MPP after degradation occurs, which indicates the device stability measured at MPP should be actually longer than what is reported here.

ASSOCIATED CONTENT

Supporting Information. XRD patterns, XPS spectra, PL spectra, cross-sectional SEM image of the control and CdI₂-treated perovskite film; *J-V* curves of the PSCs based on the perovskite films treated with different amount of CdI₂. *J-V* hysteresis, EQE spectra, PCE histogram and brightness measurement of the PSCs based on control and CdI₂-treated perovskite films. This material is available free of charge via the Internet at http://pubs.acs.org.

AUTHOR INFORMATION

Corresponding Author

*jhuang@unc.edu

Notes

The authors declare no competing financial interest.

ACKNOWLEDGES

This work is financially supported by National Science Foundation under award DMR-1903981, and Air Force Office of Scientific Research (AFOSR) (Grant No. A9550-16-1-0299). W. Q. W

acknowledges the Australian Research Council (ARC) for a DECRA Fellowship (DE180101190).

REFERENCES

- (1) https://www.nrel.gov/pv/assets/pdfs/champion-module-efficiencies.20190802.pdf
- (2) Saliba, M.; Matsui, T.; Domanski, K.; Seo, J.-Y.; Ummadisingu, A.; Zakeeruddin, S. M.; Correa-Baena, J.-P.; Tress, W. R.; Abate, A.; Hagfeldt, A.; Grätzel, M. Incorporation of Rubidium Cations into Perovskite Solar Cells Improves Photovoltaic Performance. *Science* **2016**, *354*, 206-209.
- (3) Buin, A.; Comin, R.; Xu, J.; Ip, A. H.; Sargent, E. H. Halide-Dependent Electronic Structure of Organolead Perovskite Materials. *Chem. Mater.* **2015**, *27*, 4405-4412.
- (4) Eames, C.; Frost, J. M.; Barnes, P. R. F.; O'Regan, B. C.; Walsh, A.; Islam, M. S. Ionic Transport in Hybrid Lead Iodide Perovskite Solar Cells. *Nat. Commun.* **2015**, *6*, 7497.
- (5) Meggiolaro, D.; Motti, S. G.; Mosconi, E.; Barker, A. J.; Ball, J.; Andrea Riccardo Perini, C.; Deschler, F.; Petrozza, A.; De Angelis, F. Iodine Chemistry Determines the Defect Tolerance of Lead-Halide Perovskites. *Energy Environ. Sci.* **2018**, *11*, 702-713.
- (6) Liao, J. F.; Wu, W. Q.; Jiang, Y.; Zhong, J. X.; Wang, L.; Kuang, D. B. Understanding of Carrier Dynamics, Heterojunction Merits and Device Physics: towards Designing Efficient Carrier Transport Layer-Free Perovskite Solar Cells. *Chem. Soc. Rev.* **2020**, DOI: 10.1039/c8cs01012a.

- (7) Xiao, Z.; Yuan, Y.; Shao, Y.; Wang, Q.; Dong, Q.; Bi, C.; Sharma, P.; Gruverman, A.; Huang, J. Giant Switchable Photovoltaic Effect in Organometal Trihalide Perovskite Devices.

 Nat. Mater. 2014, 14, 193.
- (8) Shao, Y.; Xiao, Z.; Bi, C.; Yuan, Y.; Huang, J. Origin and Elimination of Photocurrent Hysteresis by Fullerene Passivation in CH₃NH₃PbI₃ Planar Heterojunction Solar Cells. *Nat. Commun.* **2014**, *5*, 5784.
- (9) Chen, B.; Rudd, P. N.; Yang, S.; Yuan, Y.; Huang, J. Imperfections and Their Passivation in Halide Perovskite Solar Cells. *Chem. Soc. Rev.* **2019**, *48*, 3842-3867.
- (10)Liao, J.-F.; Wu, W.-Q.; Jiang, Y.; Kuang, D.-B.; Wang, L. Maze-Like Halide Perovskite Films for Efficient Electron Transport Layer-Free Perovskite Solar Cells. *Sol. RRL* **2019**, *3*, 1800268.
- (11) Wu, W.-Q.; Liao, J.-F.; Jiang, Y.; Wang, L.; Kuang, D.-B. Bifacial Contact Junction Engineering for High-Performance Perovskite Solar Cells with Efficiency Exceeding 21%. *Small* **2019**, *15*, 1900606.
- (12) Wang, S.; Jiang, Y.; Juarez-Perez, Emilio J.; Ono, Luis K.; Qi, Y. Accelerated Degradation of Methylammonium Lead Iodide Perovskites Induced by Exposure to Iodine Vapour. *Nat. Energy* **2016**, *2*, 16195.
- (13) Berhe, T. A.; Su, W.-N.; Chen, C.-H.; Pan, C.-J.; Cheng, J.-H.; Chen, H.-M.; Tsai, M.-C.; Chen, L.-Y.; Dubale, A. A.; Hwang, B.-J. Organometal Halide Perovskite Solar Cells: Degradation and Stability. *Energy Environ. Sci.* **2016**, *9*, 323-356.

- (14) Yang, W. S.; Park, B.-W.; Jung, E. H.; Jeon, N. J.; Kim, Y. C.; Lee, D. U.; Shin, S. S.; Seo, J.; Kim, E. K.; Noh, J. H.; Seok, S. I. Iodide Management in Formamidinium-Lead-Halide-Based Perovskite Layers for Efficient Solar Cells. *Science* **2017**, *356*, 1376-1379.
- (15)Abdi-Jalebi, M.; Andaji-Garmaroudi, Z.; Cacovich, S.; Stavrakas, C.; Philippe, B.; Richter, J. M.; Alsari, M.; Booker, E. P.; Hutter, E. M.; Pearson, A. J.; Lilliu, S.; Savenije, T. J.; Rensmo, H.; Divitini, G.; Ducati, C.; Friend, R. H.; Stranks, S. D. Maximizing and Stabilizing Luminescence from Halide Perovskites with Potassium Passivation. *Nature* **2018**, *555*, 497.
- (16)Son, D.-Y.; Kim, S.-G.; Seo, J.-Y.; Lee, S.-H.; Shin, H.; Lee, D.; Park, N.-G. Universal Approach toward Hysteresis-Free Perovskite Solar Cell via Defect Engineering. *J. Am. Chem. Soc.* **2018**, *140*, 1358-1364.
- (17)Li, N.; Tao, S.; Chen, Y.; Niu, X.; Onwudinanti, C. K.; Hu, C.; Qiu, Z.; Xu, Z.; Zheng, G.; Wang, L.; Zhang, Y.; Li, L.; Liu, H.; Lun, Y.; Hong, J.; Wang, X.; Liu, Y.; Xie, H.; Gao, Y.; Bai, Y.; Yang, S.; Brocks, G.; Chen, Q.; Zhou, H. Cation and Anion Immobilization Through Chemical Bonding Enhancement with Fluorides for Stable Halide Perovskite Solar Cells. *Nat. Energy* **2019**, *4*, 408-415.
- (18) Zheng, X.; Chen, B.; Dai, J.; Fang, Y.; Bai, Y.; Lin, Y.; Wei, H.; Zeng, Xiao C.; Huang, J. Defect Passivation in Hybrid Perovskite Solar Cells Using Quaternary Ammonium Halide Anions and Cations. *Nat. Energy* **2017**, *2*, 17102.
- (19) Saidaminov, M. I.; Kim, J.; Jain, A.; Quintero-Bermudez, R.; Tan, H.; Long, G.; Tan, F.; Johnston, A.; Zhao, Y.; Voznyy, O.; Sargent, E. H. Suppression of Atomic Vacancies via

- Incorporation of Isovalent Small Ions to Increase the Stability of Halide Perovskite Solar Cells in Ambient Air. *Nat. Energy* **2018**, *3*, 648-654.
- (20)Rudd, P. N.; Huang, J. Metal Ions in Halide Perovskite Materials and Devices. *Trends Chem.* **2019**, *1*, 394-409.
- (21) Aristidou, N.; Eames, C.; Sanchez-Molina, I.; Bu, X.; Kosco, J.; Islam, M. S.; Haque, S. A. Fast Oxygen Diffusion and Iodide Defects Mediate Oxygen-Induced Degradation of Perovskite Solar Cells. *Nat. Commun.* **2017**, *8*, 15218.
- (22) Barboni, D.; De Souza, R. A. The Thermodynamics and Kinetics of Iodine Vacancies in the Hybrid Perovskite Methylammonium Lead Iodide. *Energy Environ. Sci.* **2018**, *11*, 3266-3274.
- (23) Wei, L.-y.; Ma, W.; Lian, C.; Meng, S. Benign Interfacial Iodine Vacancies in Perovskite Solar Cells. *J. Phys. Chem. C* **2017**, *121*, 5905-5913.
- (24) Wu, W.-Q.; Yang, Z.; Rudd, P. N.; Shao, Y.; Dai, X.; Wei, H.; Zhao, J.; Fang, Y.; Wang, Q.; Liu, Y.; Deng, Y.; Xiao, X.; Feng, Y.; Huang, J. Bilateral Alkylamine for Suppressing Charge Recombination and Improving Stability in Blade-Coated Perovskite Solar Cells. *Sci. Adv.* **2019**, *5*, eaav8925.
- (25) Deng, Y.; Zheng, X.; Bai, Y.; Wang, Q.; Zhao, J.; Huang, J. Surfactant-Controlled Ink Drying Enables High-Speed Deposition of Perovskite Films for Efficient Photovoltaic Modules.

 Nat. Energy 2018. 3, 560-566.
- (26) Wu, W.-Q.; Wang, Q.; Fang, Y.; Shao, Y.; Tang, S.; Deng, Y.; Lu, H.; Liu, Y.; Li, T.; Yang, Z.; Gruverman, A.; Huang, J. Molecular Doping Enabled Scalable Blading of Efficient Hole-Transport-Layer-Free Perovskite Solar Cells. *Nat. Commun.* **2018**, *9*, 1625.

- (27) Qiao, H. W.; Yang, S.; Wang, Y.; Chen, X.; Wen, T. Y.; Tang, L. J.; Cheng, Q.; Hou, Y.; Zhao, H.; Yang, H. G. A Gradient Heterostructure Based on Tolerance Factor in High-Performance Perovskite Solar Cells with 0.84 Fill Factor. *Adv. Mater.*2019, *31*, 1804217. (28) Chen, L.; Tan, Y.-Y.; Chen, Z.-X.; Wang, T.; Hu, S.; Nan, Z.-A.; Xie, L.-Q.; Hui, Y.; Huang, J.-X.; Zhan, C.; Wang, S.-H.; Zhou, J.-Z.; Yan, J.-W.; Mao, B.-W.; Tian, Z.-Q. Toward Long-Term Stability: Single-Crystal Alloys of Cesium-Containing Mixed Cation and Mixed Halide Perovskite. *J. Am. Chem. Soc.* 2019, *141*, 1665-1671.
- (29) Jiang, F.; Choy, W. C. H.; Li, X.; Zhang, D.; Cheng, J. Post-treatment-Free Solution-Processed Non-Stoichiometric NiOx Nanoparticles for Efficient Hole-Transport Layers of Organic Optoelectronic Devices. *Adv. Mater.* **2015**, *27*, 2930-2937.
- (30) Tu, Y.; Yang, X.; Su, R.; Luo, D.; Cao, Y.; Zhao, L.; Liu, T.; Yang, W.; Zhang, Y.; Xu, Z.; Liu, Q.; Wu, J.; Gong, Q.; Mo, F.; Zhu, R. Diboron-Assisted Interfacial Defect Control Strategy for Highly Efficient Planar Perovskite Solar Cells. *Adv. Mater.* **2018**, *30*, 1805085.
- (31) Yang, S.; Dai, J.; Yu, Z.; Shao, Y.; Zhou, Y.; Xiao, X.; Zeng, X. C.; Huang, J. Tailoring Passivation Molecular Structures for Extremely Small Open-Circuit Voltage Loss in Perovskite Solar Cells. *J. Am. Chem. Soc.* **2019**, *141*, 5781-5787.
- (32) Maiberg, M.; Hölscher, T.; Zahedi-Azad, S.; Scheer, R. Theoretical Study of Time-Resolved Luminescence in Semiconductors. III. Trap States in The Band Gap. *J. Appl. Phys.* **2015**, *118*, 105701.

- (33)Liao, J.-F.; Wu, W.-Q.; Zhong, J.-X.; Jiang, Y.; Wang, L.; Kuang, D.-B. Enhanced Efficacy of Defect Passivation and Charge Extraction for Efficient Perovskite Photovoltaics with A Small Open Circuit Voltage Loss. *J. Mater. Chem. A* **2019**, *7*, 9025-9033.
- (34) Jiang, Q.; Zhao, Y.; Zhang, X.; Yang, X.; Chen, Y.; Chu, Z.; Ye, Q.; Li, X.; Yin, Z.; You, J. Surface Passivation of Perovskite Film for Efficient Solar Cells. *Nat. Photon.* **2019**. *13*, 460-466.
- (35)Bu, X.; Westbrook, R. J. E.; Lanzetta, L.; Ding, D.; Chotchuangchutchaval, T.; Aristidou, N.; Haque, S. A. Surface Passivation of Perovskite Films via Iodide Salt Coatings for Enhanced Stability of Organic Lead Halide Perovskite Solar Cells. *Sol. RRL* **2019**, *3*, 1800282.
- (36)Chen, W.; Zhou, Y.; Chen, G.; Wu, Y.; Tu, B.; Liu, F.-Z.; Huang, L.; Ng, A. M. C.; Djurišić, A. B.; He, Z. Alkali Chlorides for the Suppression of the Interfacial Recombination in Inverted Planar Perovskite Solar Cells. *Adv. Energy Mater.* **2019**, *9*, 1803872.
- (37)Zheng, X.; Deng, Y.; Chen, B.; Wei, H.; Xiao, X.; Fang, Y.; Lin, Y.; Yu, Z.; Liu, Y.; Wang, Q.; Huang, J. Dual Functions of Crystallization Control and Defect Passivation Enabled by Sulfonic Zwitterions for Stable and Efficient Perovskite Solar Cells. *Adv. Mater.* **2018**, *30*, 1803428.
- (38)Lin, Y.; Chen, B.; Fang, Y.; Zhao, J.; Bao, C.; Yu, Z.; Deng, Y.; Rudd, P. N.; Yan, Y.; Yuan, Y.; Huang, J. Excess Charge-Carrier Induced Instability of Hybrid Perovskites. *Nat. Commun.* **2018**, *9*, 4981.
- (39) Yang, S.; Chen, S.; Mosconi, E.; Fang, Y.; Xiao, X.; Wang, C.; Zhou, Y.; Yu, Z.; Zhao, J.; Gao, Y.; De Angelis, F.; Huang, J. Stabilizing Halide Perovskite Surfaces for Solar Cell Operation with Wide-Bandgap Lead Oxysalts. *Science* **2019**, *365*, 473-478.

- (40) Green, M. A.; Hishikawa, Y.; Dunlop, E. D.; Levi, D. H.; Hohl-Ebinger, J.; Ho-Baillie, A.
 W. Y. Solar Cell Efficiency Tables (version 51). *Prog. Photovolt: Res. Appl.* 2018, 26, 3-12.
- (41) Wang, Q.; Shao, Y.; Dong, Q.; Xiao, Z.; Yuan, Y.; Huang, J. Large Fill-Factor Bilayer Iodine Perovskite Solar Cells Fabricated by A Low-Temperature Solution-Process. *Energy Environ. Sci.* **2014**, *7*, 2359-2365.
- (42) Han, T.-H.; Tan, S.; Xue, J.; Meng, L.; Lee, J.-W.; Yang, Y. Interface and Defect Engineering for Metal Halide Perovskite Optoelectronic Devices. *Adv. Mater.* **2019**, 1803515.
- (43) Tress, W.; Marinova, N.; Inganäs, O.; Nazeeruddin, M. K.; Zakeeruddin, S. M.; Graetzel, M. Predicting the Open-Circuit Voltage of CH₃NH₃PbI₃ Perovskite Solar Cells Using Electroluminescence and Photovoltaic Quantum Efficiency Spectra: the Role of Radiative and Non-Radiative Recombination. *Adv. Energy Mater.* **2015**, *5*, 1400812.
- (44)Zhong, J. X.; Wu, W. Q.; Liao, J. F.; Feng, W. H.; Jiang, Y.; Wang, L.; Kuang, D. B. The R ise of Textured Perovskite Morphology: Revolutionizing the Pathway toward High-Performance Optoelectronic Devices. *Adv. Energy, Mater.* **2020**, 1902256.

Table of Contents:

